Molecular Crystals and Liquid Crystals Incorporating Nonlinear Optics

Publication details, including instructions for authors and subscription information:
http://www.tandfonline.com/loi/gmcl17

Adsorption-Induced Anchoring Transitions

P. Pieranski [a] , B. Jerome [a] & M. Gabay [a]

[a] Laboratoire de Physique des Solides, Faculté des Sciences, Bât. 510, 91405, ORSAY, France

Version of record first published: 20 Apr 2011.

To cite this article: P. Pieranski , B. Jerome & M. Gabay (1990): Adsorption-Induced Anchoring Transitions, Molecular Crystals and Liquid Crystals Incorporating Nonlinear Optics, 179:1, 285-315

To link to this article: http://dx.doi.org/10.1080/00268949008055377

Mol. Cryst. Liq. Cryst., 1990, Vol. 179, pp. 285–315
Reprints available directly from the publisher
Photocopying permitted by license only

Printed in the United States of America

ADSORPTION-INDUCED ANCHORING TRANSITIONS

P. PIERANSKI, B. JEROME and M. GABAY
Laboratoire de Physique des Solides, Bât. 510, Faculté des Sciences
91405 ORSAY, France

Abstract : When a nematic/crystal interface is subjected to an exchange of particles with a reservoir of some chemical species, the anchoring **a** at this interface can be changed by varying the chemical potentials μ_i of the reanchoring substances in the reservoir.

It is shown that water is such a reanchoring substance ; anchoring transitions are observed at nematic (E9)/crystal (gypsum, muscovite, phlogopite) interfaces for critical values of the partial pressure p of water vapor in contact with the interface.

A simple theoretical model for such adsorption-included anchoring transitions is proposed.

I. THE PRINCIPLE OF ADSORPTION-INDUCED ANCHORING TRANSITIONS

The aim of the present paper is first to describe observations of several anchoring transitions, at nematic/crystal interfaces, induced by a controlled adsorption (desorption) of water (section II). The experimental facts being established clearly, the adsorption-induced anchoring transitions will be discussed in terms of a simple phenomenological model (section III).

Before entering into details of these experimental and theoretical considerations, let us expose briefly the generic idea of the adsorption-induced anchoring transition. To be more explicit we consider a nematic layer of thickness d, deposited on a surface of a solid substrate of area A (Fig. 1). The upper surface of the nematic is free i.e. in contact with a gas containing some chemical species i having chemical potentials μ_i. The anchoring phenomenon at the nematic/crystal interface is related to the structure of an interfacial layer of thickness ξ. This interfacial layer is thermodynamically described by surface variables such as the concentrations ρ_i of the chemical species, the entropy s, the internal energy u, etc...[1]. In the present case, where the liquid and the solid meeting at the interface are anisotropic, the internal

energy u is not only a function of s and ρ_i but also depends on the direction $\vec{a}$ of the nematic with respect to the crystal :

$$u = u\,(s, \rho_i, \vec{a}) \tag{I.1}$$

For a given excess entropy s and for given compositions ρ_i of the interface the anchoring direction $\vec{a}$ minimizes u. In the example of Fig. 1, the interface is subjected to heat and particle exchange with the gas (through the nematic layer) so that the anchoring direction minimizes the grand canonical potential

$$\omega = u\,(s, \rho_i, \vec{a}) - \sum_i \mu_i \rho_i - Ts \tag{I.2}$$

or

$$\omega = f(T, \rho_i, \vec{a}) - \sum_i \mu_i \rho_i \tag{I.3}$$

where $f(T, \rho_i, \vec{a}) = u\,(s, \rho_i, \vec{a}) - Ts$ is the excess free energy of the interface.

The anchoring $\vec{a}$ obtained by minimization of $\omega(T, \mu_i, \vec{a})$:

$$\left(\frac{\partial \omega}{\partial \vec{a}}\right)_{T,\mu_i} = 0 \tag{I.4}$$

must depend on μ_i and T :

$$\vec{a}_{eq} = \vec{a}(T, \mu_i) \tag{I.5}$$

Under the conditions of Fig. 1, the chemical potentials μ_i in the gas phase, assumed to be a mixture of perfect gasses, are :

$$\mu_i = kT \log p_i + \chi_i(T) \tag{I.6}$$

They can be controlled via two parameters -the temperature and the partial pressures

$$p_i = \frac{N_i}{N_{tot}}\, p \tag{I.7}$$

of individual chemical species, that is, by varying concentrations $\frac{N_i}{N_{tot}}$ for a

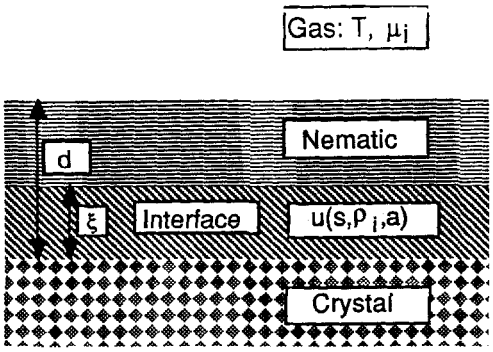

FIGURE 1, Nematic layer of thickness d deposited on a crystal surface. The nematic/crystal interface is characterized by its area A and the excess surface quantities : ρ_i -concentrations of chemical species, s-entropy, $u(s,\rho_i,\vec{a})$ -internal energy where $\vec{a}$ is the anchoring direction. The interface is subjected to heat and particle exchange with a gas reservoir of temperature T and containing chemical species at partial pressures p_i.

constant total pressure p.

Under isobaric and isothermic conditions (T = const, p = const), the only variables coupled explicitly to μ_i (p_i) are the concentration ρ_i (eq. I.2). Therefore, if any variation $\delta\vec{a}_{eq}$ follows a change $\delta\mu_i$ of the chemical potentials, it must be accompanied by some change of $\delta\rho_i$ of the surface concentrations ρ_i.

This statement can be considered as a practical definition of adsorption (desorption)-induced effects on anchoring.

The temperature and the partial pressures cannot be arbitrary but, obviously, under the conditions of Fig. 1, must be in the range of existence of the gas phase ; independently of what can happen at the interface, the space of the intensive variables (T, μ_i) is already divided into domains of different 3D phases. For simplicity, let us suppose that the gas contains only water. Then the corresponding space is a plane (T,p) shown in Fig. 2a and it is divided by phase transition lines.

In general, to each point (T,p) inside the gas domain corresponds an

anchoring $\vec{a}(T,p)$ which can be represented as a point on a unit sphere. A trajectory in phase space is then modeled by an evolution of $\vec{a}(T,p)$ on the sphere.

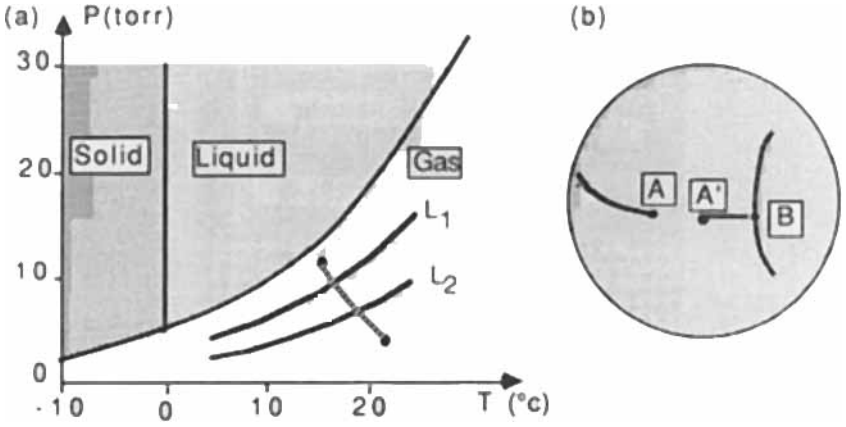

FIGURE 2, Definition of anchoring transition induced by adsorption of water. a) - Phase diagram of water. In the geometry of Fig. 1, the domain of the vapor phase has to be explored in the search for anchoring transitions. L_1 and L_2 are hypothetical lines of anchoring transitions of, respectively, 1st and 2nd order. b) - Trajectories of the anchoring $\vec{a}(p,T)$ corresponding to a path in the (p,T) plane crossing the transitions lines L_1 and L_2.

In addition to smooth variations of the anchoring $\vec{a}$ as a function of (p,T), one can expect two types of singularities to occur on trajectories $\vec{a}(T,p)$:

- First-order anchoring transitions : The anchoring jumps from A to A' (Fig. 2b) when the path in the (T,p) space crosses a first-order anchoring transition line L_1 (Fig. 2a). Such a line can terminate by a critical point (or can join other lines at multicritical points).
- Second-order anchoring transition : The anchoring trajectory can bifurcate at point B (Fig. 2b) when the path in the (T,p) plane crosses a second-order anchoring transition line L_2.

The first-order anchoring transitions induced by adsorption of water has been demonstrated by recent experiments[2]. In the next section, we will report on more recent and extensive experiments.

II. EXPERIMENTAL

II.1. Set-up

A scheme of the experimental set-up is shown in Fig. 3. A sample (S),i.e. a thin crystal plate ($\approx$ 1 x 1 cm) with a thin (few μm) nematic (E9) layer spread on top of it, is mounted in the middle of a h = 4 mm-thick brass cell bordered, in its central part, by glass windows W and having profiled inlet and outlet ducts. The temperature of the cell is regulated by thermoelectric chips.

The cell is fixed on the rotating table of a polarizing microscope equipped with a Babinet-Soleil compensator (B-S). The analyzer and polarizer of the microscope are crossed and coupled mechanically in order to allow their simultaneous rotation in the crossed position. After the compensation of the birefringence of the crystal plate itself, the direction of the nematic molecules is determined simply from extinctions. The gas composition i.e. the partial pressure p_{H_2O} of the water vapor in nitrogen is regulated using a simple device. Its principle is based on mixing of two, one dry and the second water vapor saturated, streams of nitrogen i_o and i_s. The water vapor pressure $p_{H_2O} = \tilde{p}.p_s$ of the resulting mixture is :

$$p_{H_2O} = \frac{i_s}{i_o+i_s}.p_s = \tilde{p}.p_s \qquad \text{(II.1)}$$

In practice, a finite time is needed for recovery of thermodynamic equilibrium after a change of the partial pressure P_{H_2O} resulting from a modification of settings of coupled valves V_0 and V_s. The recovery of equilibrium involves vapor diffusion in the volume of the cell chamber and diffusion of water molecules, through the nematic layer, to (or from) the nematic-substrate interface.

The time constants for diffusion of water in the gas in the cell (equilibration of p_{H_2O} in the cell volume) τ_{cell} and through the nematic layer τ_{nem} can be estimated from corresponding characteristic lengths, $\frac{h}{2} \simeq 2$ mm and $d \simeq 10$ μm, and diffusion constants $D_{H_2O/air} \approx 0.24$ cm^2/sec., $D_{H_2O/nem} \approx 10^{-5}$. cm^2/sec :

$$\tau_{cell} \approx \frac{4.10^{-2}}{0.2} = 0.2 \text{ sec}$$

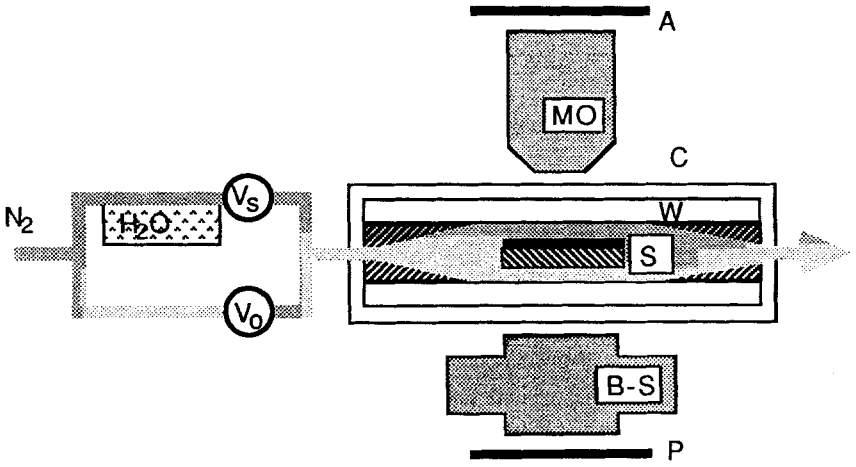

FIGURE 3, Experimental set-up : S-sample, C-cell equiped with glass windows W, B-S.- Babinet-Soleil compensator, A and P- Analyzer and polarizer coupled mechanically, V_0 and V_s- valves, MO- Microscope objective.

and (II.2)

$$\tau \sim \frac{10^{-6}}{10^{-6}} \sim 1 \text{ sec.}$$

On the time scale of observed anchoring transitions, i.e. the time needed for domain walls to move across the sample which, typically, for a supersaturation of few percent is of the order of 10 sec., these two characteristic times are fairly small and can be neglected.

II. 2. Crystal surfaces

The orienting action of crystal surfaces on nematics is known since the pioneering work of Grandjean and Mauguin[3-4].

In the present studies we have used minerals providing perfect cleavages and available in form of large monocrystals -gypsum and several micas. The crystals were cleaved in air and only freshly cleaved surfaces were used in experiments. Although various minerals have been widely used in studies of anchorings[5], little attention was paid to their structures. The aim of the next two sections is to provide essential information about gypsum and two types of mica crystals.

Gypsum (Ca $S0_4$ $2H_2O$) : Gypsum crystals have symmetry C_{2h}^6 [6]. Some symmetry elements of this space group are represented in Fig. 4a. The unit cell (a,b,c) is a monoclinic prism with a rectangular base ($\vec{a} \perp \vec{b}$) and tilted in the ($\vec{a}$, $\vec{c}$) plane. The twofold axes (of normal and screw type) are parallel to the [010] direction. The glide plane Σ is normal to [010].

The structure of this mineral[6] can be seen as a stack of triple layers ; each triplet is made of a Ca $S0_4$ sheet bordered by two H_20 sheets. The cohesion forces between the triplets in the stack arise from hydrogen bonds between water layers. As expected from such a structure, the cleavage of the gypsum crystal takes place along Σ planes and provides surfaces with a twofold (C_2) symmetry.

Micas[7] : The case of mica is much more complicated because its composition and consequently its structure, varies considerably. In this paper we consider only two varieties of mica :

- the muscovite mica of composition K Al_2 $[(Si_3Al)\ 0_{10}\ (OH,F)_2]$, and
- the phlogopite mica of composition K Mg_3 $[(Si_3Al)\ 0_{10}\ (OH,F)_2]$.

They are typical members of two structural classes of mica -dioctahedral and trioctahedral.

In order to understand the meaning of this classification and its importance for studies of anchorings, it is useful to represent the architecture of micas in several steps :

1° Consider an elementary sheet of composition $[Si_20_5]^{2-}$ made of SiO_4 tetrahedra sharing corners as shown in Fig. 5a. The oxygen ions O^{2-} sheared by the tetrahedra are organized into a Kagome lattice. The oxygen ions situated at the top of the tetrahedra, known as apical oxygens, form a hexagonal lattice of symmetry C_{6v}.

2° Place OH^- or F^- ions in centers of the hexagons formed by the apical oxygens ; the hexagonal lattice resembles now a triangular lattice (Fig. 5b).

3° Take two identical $[(Si_20_5)\ (OH,F)]^{3-}$ layers facing their apical oxygen sheets and shift one with respect to the other by $\vec{l}$ as shown in Fig. 5c. The shift creates three octahedral cavities (per each hexagon) between the two layers. In the phlogopite all of these three cavities are filled with Mg^{2+} ions while in the muscovite only two of the three cavities are filled with Al^{3+} ions. Because of the shift $\vec{l}$ the hexagonal symmetry C_{6v} is "slightly" broken to C_{2v} in the mica phlogopite. In the mica muscovite the departure

from the hexagonal symmetry is much more pronounced. The broken symmetry is characterized by the vector $\vec{l}$; because of the initial C_{6v}

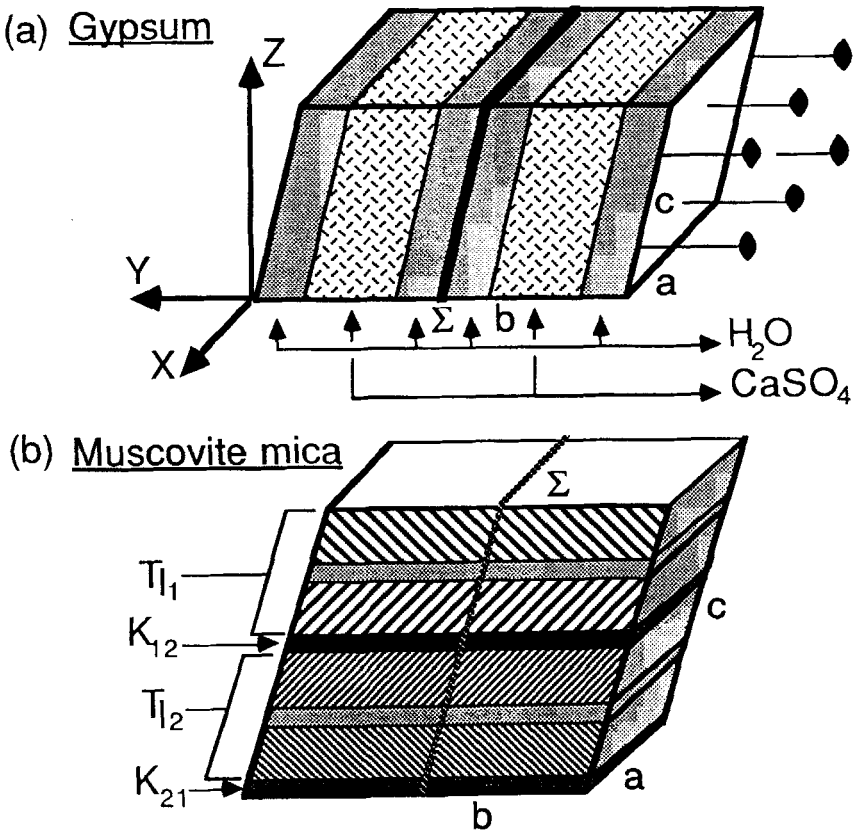

FIGURE 4, Schematic representations of the structures of the gypsum (a) and of the muscovite mica (b) having the same symmetry C_{2h}^6. The unit cell is monoclinic, Σ is the glide plane, the twofold axes are perpendicular to Σ.

symmetry, six equivalent staggering vectors are possible. Each triple layer of composition Al_2 (or Mg_3) $[(Si_4O_{10})$ (OH,F)] can be briefly noted $T_{\vec{l}}$.

4° Such triplets are electrically neutral and their stacks would be extremely easy to cleave. In fact, this is the case for talc. In the two micas of interest here, one of the four silicon ions Si^{4+} is substituted, at random, by an aluminum ion Al^{3+}. In order to compensate this charge, the triplets $T_{\vec{l}}^{-}$ are

intercalated by K^+ ions.

The structure of muscovite mica of symmetry C_{2h}^6 is a stack of triplets :

$$\ldots T_{\vec{l}_1}^{-} K_{12}^{+} T_{\vec{l}_2}^{-} K_{21}^{+} T_{\vec{l}_1}^{-} \ldots$$

shown in Fig. 4b. The staggering vectors $\vec{l}_1$ and $\vec{l}_2$ are symmetrical with respect to the glide plane Σ and form an angle $(\vec{l}_1, \vec{l}_2)$ of 120°.

The cleavage of mica consists in separating two adjacent triplets ; the intercalating potassium ions must be equally divided between the two surfaces created by the cleavage. It seems that the distribution of the potassium ions on cleaved surfaces is random[8]. In such a case, the cleaved surface must resemble the Kagome lattice made of oxygens with one half of holes in it filled at random by potassium ions.

Because of the internal structure of the triplet adjacent to the surface, the Kagome lattice is distorted. This distortion is very small in the phlogopite mica (Fig. 6a) and much larger in the muscovite mica (Fig. 6b).

Strictly speaking, the surface of the muscovite mica of symmetry C_{2h}^6 must be symmetryless because there are no symmetry axes perpendicular to it. The cleavage can take place either in the plane K_{12} or in the plane K_{21} (Fig. 4b). The respective structures of obtained surfaces must be symmetric with respect to the reflexion in the mirror plane Σ.

II.3 Anchoring transitions

II.3.a. Three mechanisms of the first order anchoring transitions

The anchoring transitions described in the following sections are all first-order and involve a discontinuous change $\Delta\varphi$ of the azimuthal angle of the anchoring. Let $\tilde{p}_c$ be the critical vapor pressure, and let φ_u ($\tilde{p} > \tilde{p}_c$) and φ_b ($\tilde{p} < \tilde{p}_c$) be the azimuthal angles above and below the transition.

The transition from the parental orientation, say φ_b, to the new orientation φ_u is initiated by defects of three types. One can use this fact for a classification of different mechanisms of the anchoring transitions of first-order :

1° surface point defects : Domains with the new orientation φ_u nucleate and grow in a matrix of the parental orientation φ_b. This mechanism is illustrated by the photograph in Fig. 7. When the transition is crossed back and forth several times, the domains always nucleate at the same

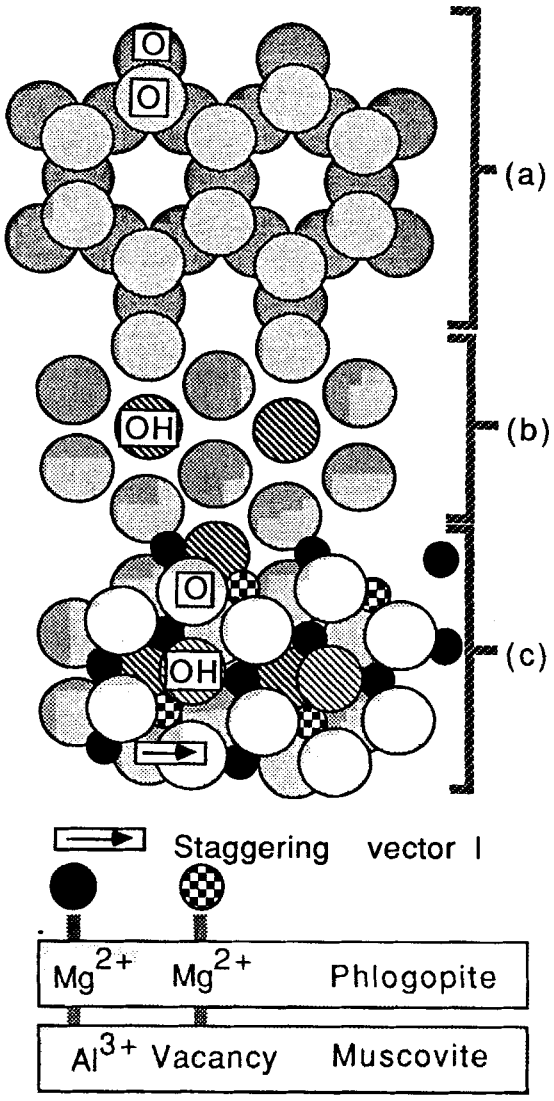

FIGURE 5, Structure of phyllosicates : a) - ideal $[Si_2O_5]^{2-}$ sheet, b) - apical oxygens form a hexagonal lattice centered by OH^- or F^- ions, c) - three octahedral cavities are formed by staggering ($\vec{l}$) of two adjacent $[(Si_2O_5)(OH,F)]^{3-}$ sheets.

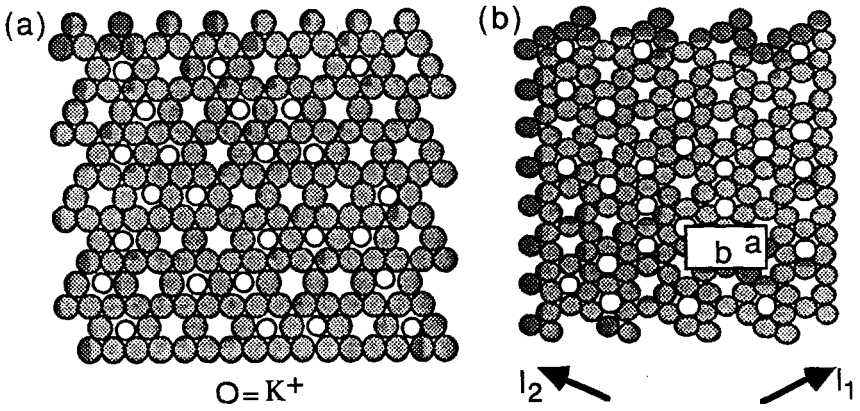

FIGURE 6, Ideal surfaces created by cleavage : a) phlogopite : oxygens form a Kagome lattice, potassium ions are distributed at random. The hexagonal symmetry of the Kagome lattice is slightly broken due to the staggering $\vec{l}$ inside the triplet $T_1^{\rightarrow}$ adjacent to the surface ; b) muscovite : the Kagome lattice is strongly distorted because one of the three octohedral cavities inside the surface triplet is left empty. Additional breaking of the symmetry is due to interactions with the bulk of the crystal. $\vec{l}_1$ and $\vec{l}_2$ are alternating staggering vectors in the stack.

points on the surface which obviously must correspond to various point defects (for example dust particles). The structure of walls surrounding the domains is visualized in Fig. 8. The walls can be of two types, W_A and W_B. In the wall W_A, the bisecting line A (between φ_u and φ_b) is one of intermediate directions in the wall. In the wall W_B the intermediate direction is along the bisecting line B.

2° surface walls (Fig. 9) The new orientation φ_u preexists in a π-surface wall when the wall is present in the parental phase. The transition takes place by splitting of the wall into the two subwalls W_A and W_B, which move apart.

3° bulk disclinations (Fig. 10) When a bulk π-disclination is present in the sample close to the crystal surface, it can stick to the surface where it is transformed into a π-wall, which splits into the two subwalls, as in the previous case.

See Color Plate I.

FIGURE 7, First mechanism of an anchoring transition : typical domains with a new orientation φ_u nucleating and growing in the matrix with the parental orientation φ_b.

In all these cases, when the anchoring transition occurs, the parental anchoring coexists with the new anchorings (the motion of walls can always be slowed down by an appropriate setting of the vapor pressure $\tilde{p}$). The discontinuity $\Delta\varphi = \varphi_u - \varphi_b$ is then obvious to measure.

II.3.b. *E9/gypsum interface*

As shown in section II.2, only one kind of surface is produced by the cleavage

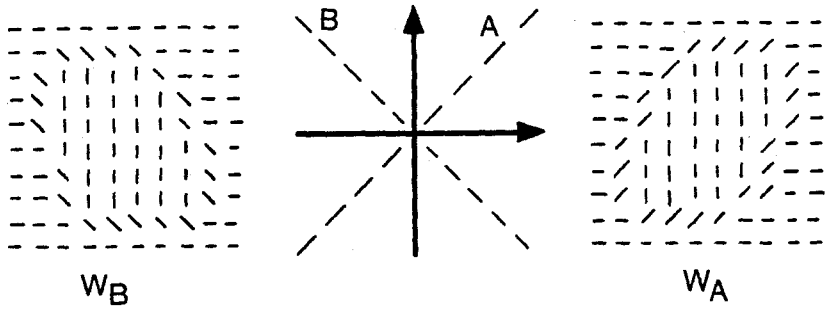

FIGURE 8, Two types of walls WA and WB are possible. Usually their shapes are elliptic. WA and WB ellipses are oriented differently.

of the gypsum. In agreement with this theoretical prediction, the anchoring on the gypsum surface is always uniform. Its direction varies as a function of the

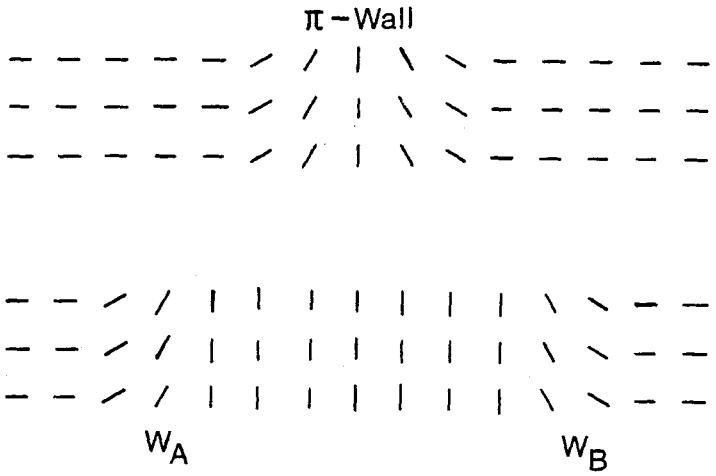

FIGURE 9, Second mechanism of a 1st-order anchoring transition : a surface π-wall splits into two subwalls WA and WB ; a band with the new orientation is created.

water vapor pressure as shown in Fig. 11. The angle φ is defined in Fig. 11 with respect to a normal to the edge of the gypsum plate. At ambient temperature (T = 20° C), the first-order anchoring transition occurs for $\tilde{p}_c$

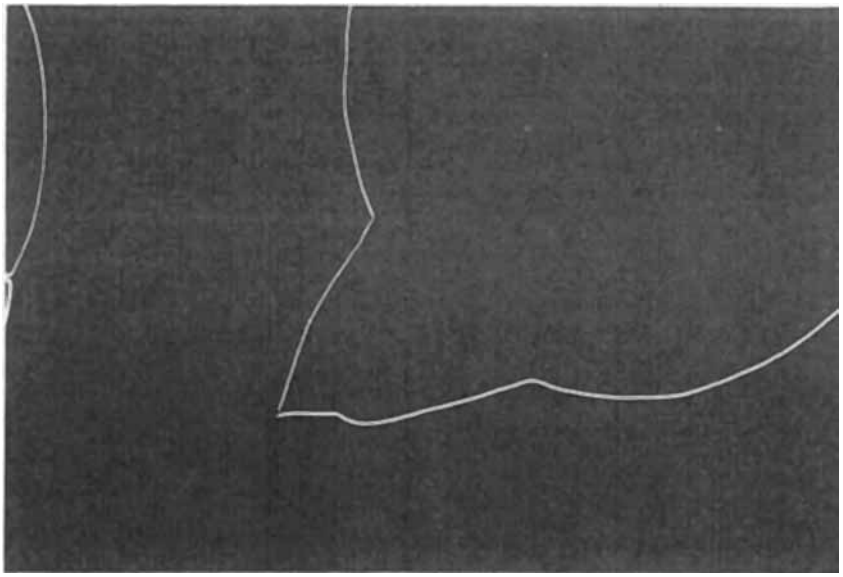

See Color Plate II.

FIGURE 10, Third mechanism of 1st-order anchoring transitions : a bulk π-disclination sticks to the crystal surface where it transforms into a surface π-wall. The π-wall splits into the subwalls as in Fig. 9.

$= 0.75$. The corresponding discontinuity is $\Delta\varphi = 82°$.

The domains with the new orientation $\vec{a}'$ growing in the matrix of orientation $\vec{a}$ are irregular in shape ; their walls are frequently pinned by some irregularities of the cleavage plane.

The anchoring transition as well as the whole plot $\varphi(\tilde{p})$ are very reproducible from sample to sample and over a long time period (a few weeks).

II.3.c. *E9/muscovite*

Cleavage surfaces of the mica muscovite are usually divided into large fields corresponding to the two types of possible cleavage levels (K_{12} or K_{21})[9]. The existence of these fields is illustrated in Fig. 12. The anchoring in these fields is symmetrical with respect to the glide plane Σ.

The azimuthal angle φ measured with respect to the glide plane Σ (the axis N_p of the low refractive index of the crystal plate) varies as a function of $\tilde{p}$ as shown in Fig. 13. There are three anchoring transitions :

- The first transition involves a discontinuity $\Delta\varphi_1 = 90°$. This transition is illustrated in Fig. 12. The domains growing in dark fields are also dark

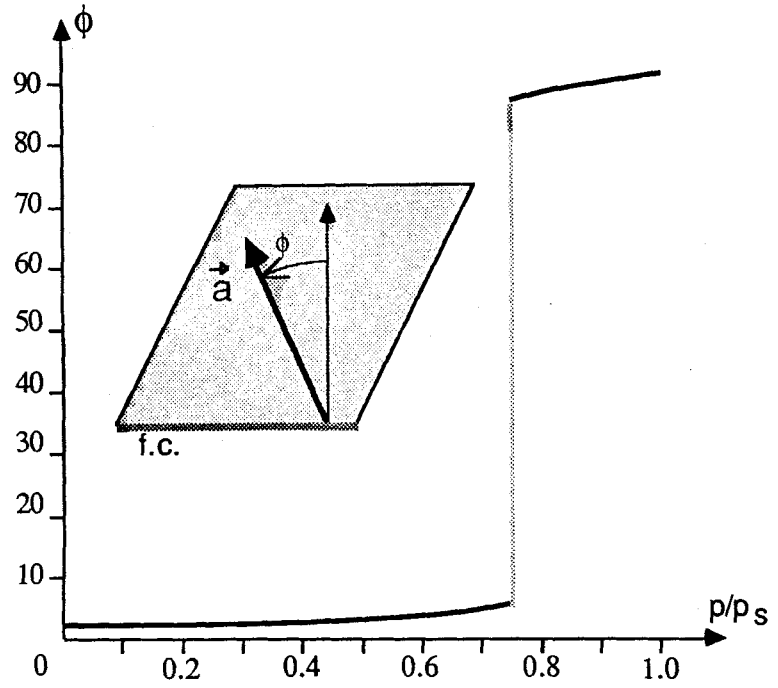

FIGURE 11, E9/gypsum interface : variation of the anchoring direction φ as a function of the water vapor pressure $\tilde{p} = p/p_s$. Definition of the azimuthal angle φ is shown in the insert. f.c. is the edge of the crystal plate corresponding to the fibrous cleavage[9].

which means that the new orientations must be orthogonal with respect to the parental orientations.

- The second transition involves a discontinuity $\Delta\varphi_2 = 60°$. It is illustrated in Fig. 14. In this example the surface π-wall splits into two subwalls. The domain with the new orientation, growing in the bright field, is dark ; the new orientation is the same as the parental orientation in the dark field.

- The third anchoring transition is inverse to the previous one. The anchoring returns back to its second orientation : $\vec{a}_4 = \vec{a}_2$.

The orientations of the four anchorings with respect to the distorted Kagome lattice are shown in Fig. 15.

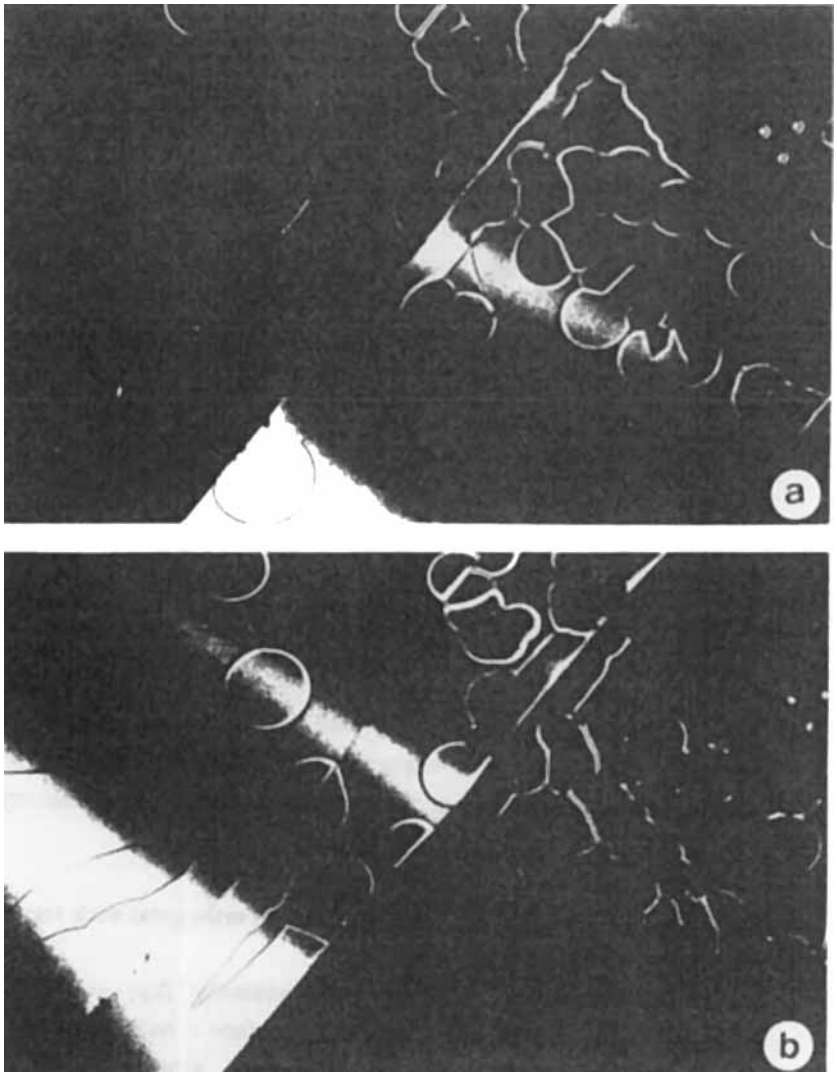

FIGURE 12, The first anchoring transition in the two fields on a surface of muscovite mica : the anchorings in these fields are symmetric with respect to the glide plane Σ. a) For a proper orientation of crossed polarizers, the field on the left of the photograph is extinguished. The new orientation $\vec{a_2}$ in the interior of growing domains is at right angle to the parental anchoring $\vec{a_1}$. b) The field on the right side of the photograph can also be extinguished after a rotation of crossed polars by 60°.

See Color Plate III.

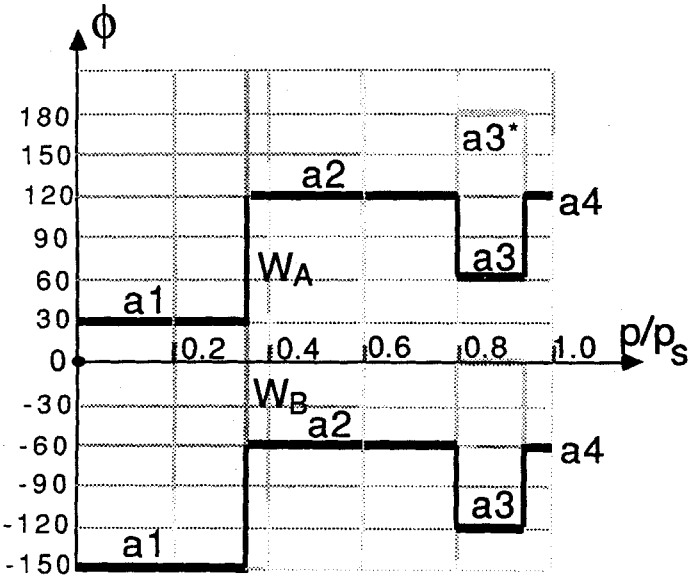

FIGURE 13, Variation of the anchoring at a E9/muscovite interface as a function of the partial pressure $\tilde{p}_{H_2O}$. Heavy and light horizontal lines represent respectively stable and metastable anchorings. (The walls mediating the anchoring transitions involve continuous variation of the angle φ). The heavy and light vertical lines connecting such two horizontal lines represent, respectively, low and high energy domain walls mediating the anchoring transition.

II.3.d. *E9/phlogopite*

Only one anchoring transition occurs at $\tilde{p}_c = 0.5$. For $\tilde{p} < \tilde{p}_c$, three anchorings coexist on a typical cleavage surface. Their directions are visualized in Fig. 16. The transition involves a discontinuity $\Delta\varphi = \bullet\ 30°$; the three new anchorings bisect angles between the three precedent.

II.3.e. *Behavior of domain walls*

In order to illustrate motions of domain walls during an anchoring transition, we took a multiple-exposure photograph (Fig. 17). The photograph shows positions of domain walls recorded every 10 seconds after the beginning of the anchoring transition (E9/muscovite interface, first anchoring transition).

From successive configurations of domain walls one can deduce that :

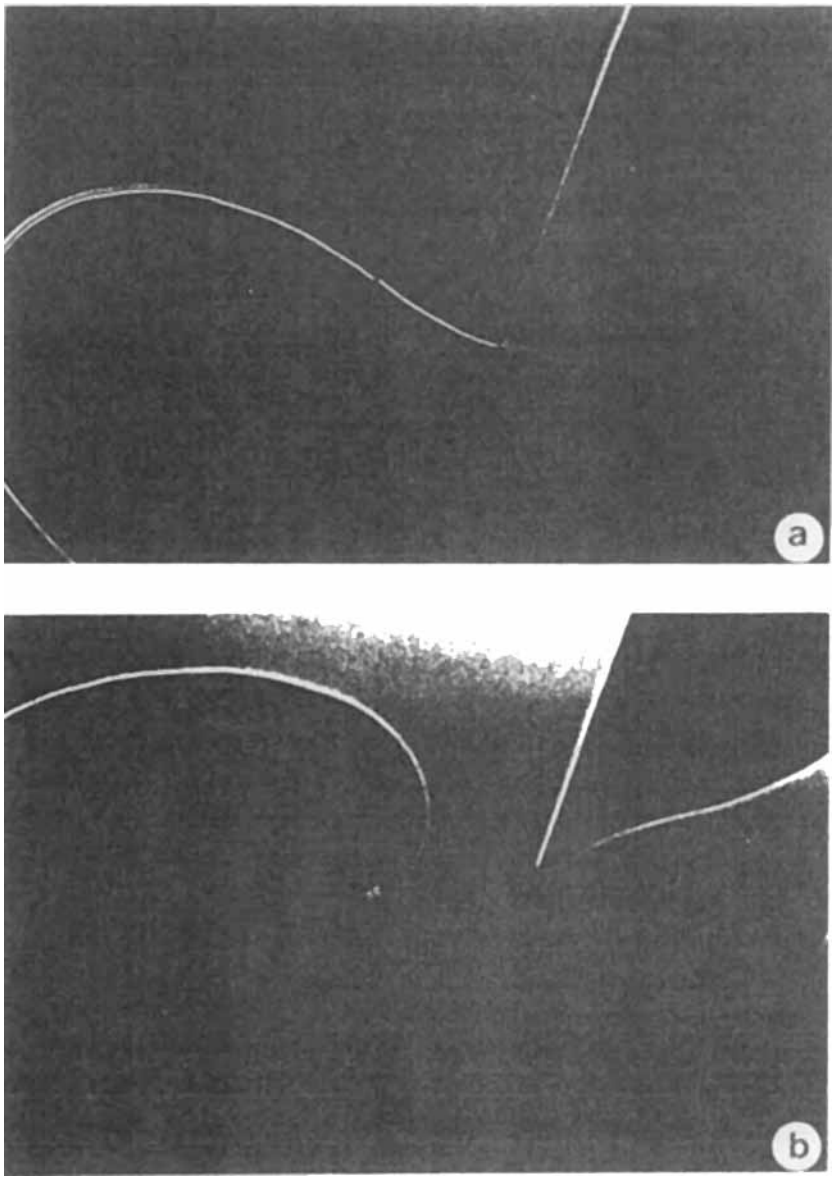

FIGURE 14, The second anchoring transition at a E9/muscovite interface : a) a π-wall preexists in fields with parental orientations ; b) the π-wall splits at the transition.

See Color Plate IV.

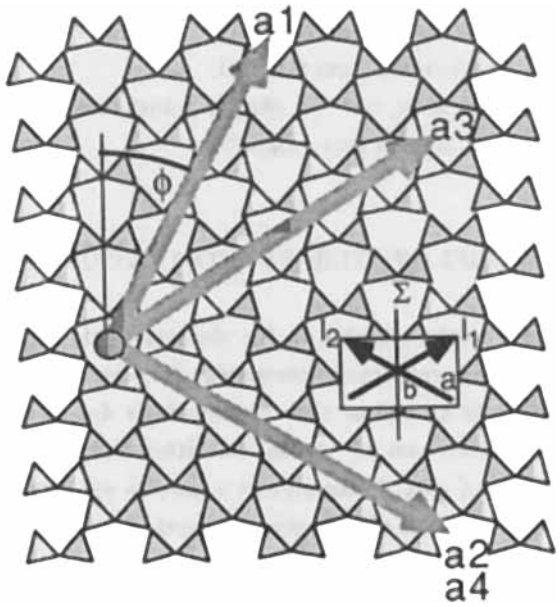

FIGURE 15, E9/muscovite interface : orientation of the four anchorings with respect to the structure of the crystal surface.

FIGURE 16, Orientations of anchorings at E9/phlogopite interface. The light arrows indicate anchoring directions above the anchoring transition that occurs for $\tilde{p}_c \approx 0.5$.

1° When two domain walls of the same type come into contact they coalesce.

2° When the domain walls of different type (W_A and W_B) meet they do not coalesce but associate and form a π-wall.

On a longer time scale, one can observe transformations of such π-walls into bulk π-disclination loops that collapse.

III. SIMPLE MODEL OF ANCHORING TRANSITIONS

The experimental results reported in the previous sections raise a number of fundamental questions concerning interactions between the nematic phase and the crystal substrate as well as their modifications due to the adsorption of water. These problems can be approached either from microscopic or from macroscopic points of view. In the present paper, we will discuss the anchoring transitions mainly in terms of a phenomenological model.

As stated in section I., any isothermal change $\delta\dot{a}$ of the anchoring, induced by a modification $\delta\mu_{H_2O}$ of the chemical potential of the water vapor, must be accompanied by some change $\delta\rho_{H_2O}$ of the excess surface concentration (the subscript H_2O will be emitted in order to simplify notations).

One can distinguish two cases :

1° The anchoring transition is only a by-side product of layered adsorption. In other terms, the discontinuity $\Delta\rho$ could occur even if the liquid layer was not nematic but just isotropic. In such a case, the anisotropy of the nematic phase would only modify the amplitude of the discontinuity $\Delta\rho$.

2° The anisotropy of the liquid crystal is essential for the occurrence of the discontinuity $\Delta\rho$. The evolutions of the anchoring $\varphi(\mu,T)$ and of the density $\rho(\mu,T)$ are intimately connected ; the singular behavior of one of these quantities is impossible in the absence of any singularity of the second.

We cannot now discriminate between these two possibilities in connection with any of reported anchoring transitions.

In spite of this uncertainty, it seems more attractive to develop the second hypothesis, which is more original. Indeed, the first possibility would involve only modifications of otherwise extensively discussed theory of multilayer

FIGURE 17, Motion of domain walls at a E9/muscovite interface. Multiple-exposure photograph. Note coalescence of walls of the same type and creation of π-walls when walls of different types colide.
See Color Plate V.

adsorption[10]. The distinction between the two possible models appears at the very beginning of the model.

When the excess free energy $f_{tot}(T,\rho,\varphi)$ is considered, one can separate the isotropic and anisotropic parts :

$$f_{tot}(T,\rho,\varphi) = f_{iso}(T,\rho) + f_a(T,\rho,\varphi) \qquad \text{(III.1)}$$

According to the second possibility, the density $\rho_{iso}(\mu,T)$ whould vary linearly near the transition occurring for $\mu = \mu_c$. This assumption is satisfied

by writing :

$$f_{iso}(\tilde{\rho},T) = \frac{1}{2a}\tilde{\rho}^2 + \mu_c\tilde{\rho} \tag{III.2}$$

where $\tilde{\rho} = \rho - \rho_c$ and $a > 0$. From (III.2), one gets :

$$\mu_{iso} = \frac{\partial f}{\partial \tilde{\rho}} = \frac{1}{a}\tilde{\rho} + \mu_c \tag{III.3}$$

or

$$\tilde{\rho} = a\,\tilde{\mu}_{iso} \tag{III.4}$$

The anisotropic part f_a of the free energy must now depend on the angle φ between the anchoring (supposed to be planar) and some special direction on the crystal surface. It can be expanded into a Fourier series :

$$f_a = \sum_m [a_m(\tilde{\rho},T)\cos m\varphi + b_m(\tilde{\rho},T)\sin m\varphi] \tag{III.5}$$

where m must be even ($\vec{n} = -\vec{n}$)

In order to simplify next considerations we will limit the series to the first two terms compatible with the C_{2v} symmetry (approximating the surface of the muscovite). We will also suppose that the anchoring transition is due to a change of sign of the cos 2φ term when the excess density of adsorbed water molecules passes through the critical value ρ_c (i.e. when $\tilde{\rho} = 0$).

With such simplifications one gets :

$$f_a = \alpha_2(T)\tilde{\rho}\cos 2\varphi + a_4(T)\cos 4\varphi \tag{III.6}$$

where $\alpha_2(T) > 0$.

From the expression of $f_{tot} = f_{iso} + f_a$, we can calculate the grand canonical potential :

$$\omega_{tot} = f_{tot} - \rho\,\mu \tag{III.7}$$

From :

$$\tilde{\mu} = \frac{\partial f_{tot}}{\partial \tilde{\rho}} - \mu_c = \frac{1}{a}\tilde{\rho} + \alpha_2 \cos 2\varphi \qquad \text{(III.8)}$$

one gets :

$$\tilde{\rho} = a(\tilde{\mu} - \alpha_2 \cos 2\varphi) \qquad \text{(III.9)}$$

By substituting (III.9), (III.2) and (III.6) into (III.7), one gets :

$$\omega = -\frac{1}{2} a \tilde{\mu}^2 + \tilde{\mu}(a\,\alpha_2 \cos 2\varphi - \rho_c) + (a_4 - \frac{1}{4} a\alpha_2^2) \cos 4\varphi - \frac{1}{4} a\alpha_2^2 - \mu_c \rho_c \qquad \text{(III.10)}$$

This thermodynamic potential can be separated into two parts as follows :

$$\omega = \omega_{iso}(\tilde{\mu}) + \omega_a(\tilde{\mu}, \varphi)$$

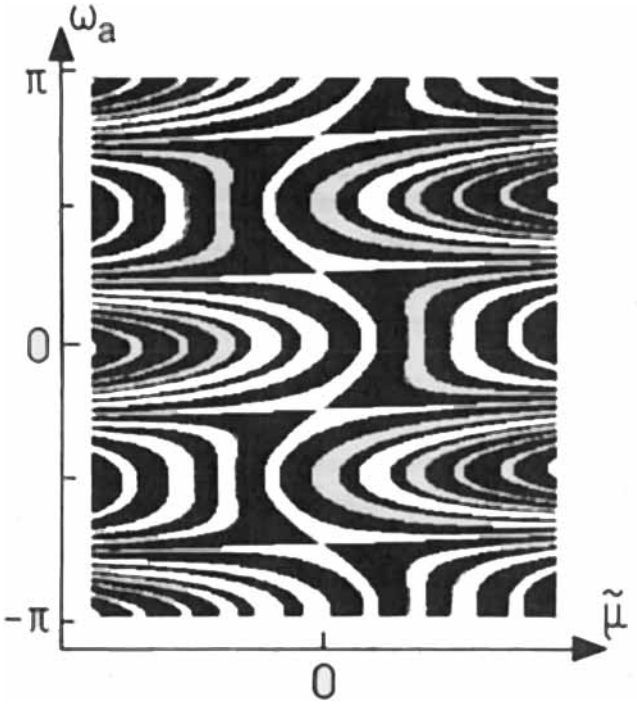

FIGURE 18a, Anisotropic part of the grand canonical potential characteristic of a 1st-order anchoring transition.
See Color Plate VI.

In the search for minima defining equilibrium states, only the anisotropic part $\omega_a(\tilde{\mu}, \varphi)$ is pertinent, since the chemical potential $\tilde{\mu}$ is fixed by the gas reservoir and the isotropic contribution $\omega_{iso}(\tilde{\mu})$ is independent of φ.

The detailed shape of the anisotropic term $\omega_a(\tilde{\mu}, \varphi)$, plotted in Fig. 18, depends on the sign of $\bar{a}_4 = (a_4 - \frac{1}{4} a\, \alpha_2^2)$.

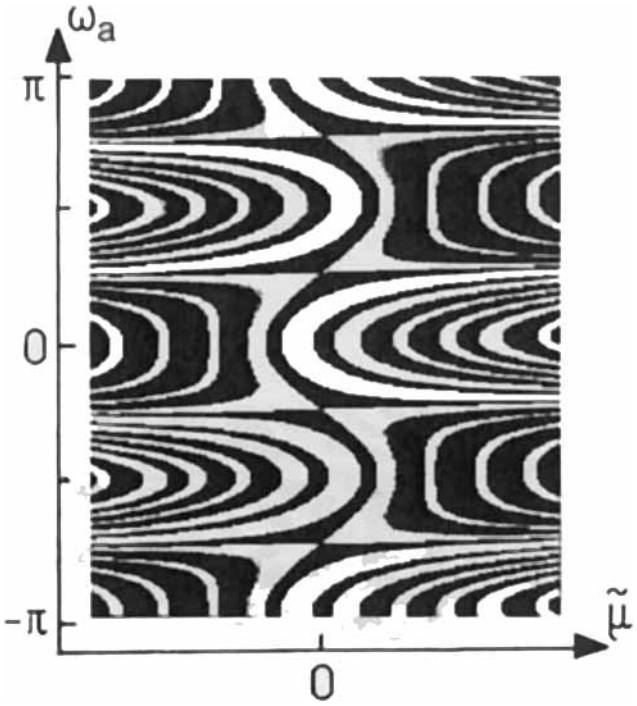

FIGURE 18b, Anisotropic part of the grand canonical potential characteristic of a 2nd-order anchoring potential.
See Color Plate VII.

- $\bar{a_4} < 0$: first-order anchoring transition (Fig. 18a)

For $\tilde{\mu} < 0$, the deepest valleys are located at $\varphi = 0, \pm \pi$ while for $\tilde{\mu} > 0$ they are located at $\varphi = \bullet \frac{\pi}{2}, \ldots$ (see also Fig. 20a).

At the transition point $\tilde{\mu} = 0$, the height of the barrier separating those valleys is $\Delta\omega = |2\bar{a}_4|$.

In the presence of some supersaturation, i.e. for $\tilde{\mu} > 0$ the height of the

barrier goes down with $\tilde{\mu}$ and disappears for $\tilde{\mu}_+ \geq -4\frac{\bar{a}_4}{a\alpha_2}$; this is the spinodal limit of this first-order anchoring transition (Fig. 20a).

The discontinuous variation of the density $\tilde{\rho} = \rho - \rho_c$, characteristic of this transition, is shown in Fig. 19a.

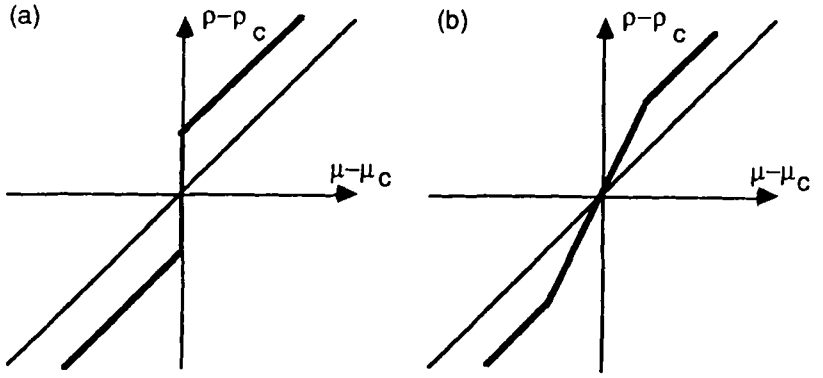

FIGURE 19, Variation of the density ρ as a function μ : a) 1st-order anchoring transition ; b) 2nd-order anchoring transition.

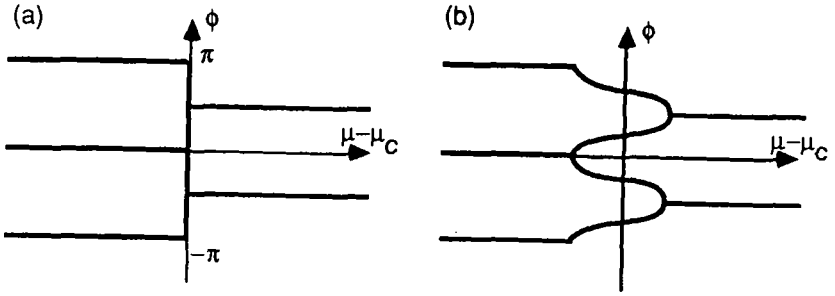

FIGURE 20, Variation of the azimuthal angle φ as of function of μ : a) 1st-order anchoring transition ; b) 2nd-order anchoring transition.

- $\bar{a}_4 > 0$: second-order anchoring transition (Fig. 18b)

Instead of one first-order transition occurring for $\tilde{\mu} = 0$, it is clear from the plot that two second-order anchoring transitions will take place ; one for $\tilde{\mu}_- = -4\frac{\bar{a}_4}{a\alpha_2}$ and the second for $\tilde{\mu}_+ = 4\frac{\bar{a}_4}{a\alpha_2}$.

If one starts with $\tilde{\mu} < -4\frac{\bar{a}_4}{a\alpha_2}$ in the valley $\varphi = 0$ then, for $\tilde{\mu}$ increasing, this valley is followed until $\tilde{\mu}$ reaches the critical value $\tilde{\mu} = -4\frac{\bar{a}_4}{a\alpha_2}$. Here, the valley $\varphi = 0$ bifurcates (see Fig. 20b). The angle $\varphi(\tilde{\mu})$ corresponding to the two branches is given by :

$$\cos 2\varphi = -\tilde{\mu}\frac{\alpha_2 a}{4\bar{a}_4} \tag{III.11}$$

The corresponding density variation :

$$\tilde{\rho} - a\tilde{\mu} = [(a\alpha_2)^2/4\bar{a}_4]\tilde{\mu} \tag{III.12}$$

is shown in Fig. 19b.

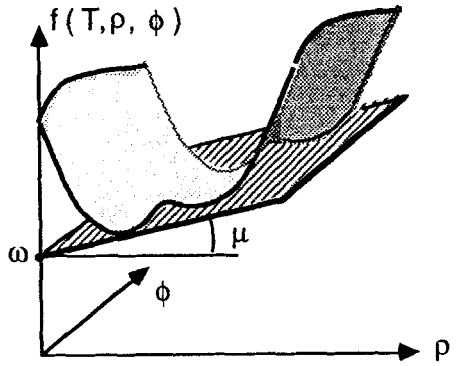

FIGURE 21, Geometrical construction giving equilibrium values of $\tilde{\rho}$ and φ corresponding to the chemical potential $\tilde{\mu}$ fixed by the vapor reservoir.

An alternative discussion can be followed using the free energy f_{tot} : for a chemical potential $\tilde{\mu}$ set by the gas reservoir, the equilibrium values of $\tilde{\rho}$ and φ are found by osculating the surface $f_{tot}(\tilde{\rho}, \varphi)$ with a plane P parallel to the φ axis, tangent to the surface f_{tot} and having the slope μ (Fig. 21). It is equivalent and easier to osculate the surface $\bar{f}_{tot} = f_{tot} - \mu_c\tilde{\rho}$ with a plane $\bar{P}$

having the slope $\tilde{\mu}$.

The conformation of the surface $\tilde{f}_{tot}$ and consequently the points of contact of the plane $\bar{P}$ with this surface depends on the sign of $\bar{a}_4$:

- $\bar{a}_4 < 0$: The function $\tilde{f}_{tot}$ plotted in Fig. 22a has the shape of a valley (due to the f_{iso} term) corrugated by the anisotropic term f_a. These corrugations can be seen as two rows of minima : one row for $\tilde{\rho} = -a\alpha_2$ with minima located at $\varphi = 0, \pm \pi, \bullet 2\pi,...$ and the second row for $\tilde{\rho} = a\alpha_2$ with the minima located at $\varphi = \pm \frac{\pi}{2}, \bullet \frac{3\pi}{2},...$

For $\tilde{\rho} < -a\alpha_2$ and $\tilde{\rho} > a\alpha_2$, there are some grooves located at $\varphi = 0, \bullet \pi, \pm 2\pi,...$ for $\tilde{\rho} < -a\alpha_2$ and $\varphi = \pm \frac{\pi}{2}, \pm \frac{3\pi}{2},...$ for $\tilde{\rho} > a\alpha_2$.

Then, the plane $\bar{P}$ is tangent to the surface $\tilde{f}_{tot}$ for $\tilde{\mu} < 0$ at :

$$\tilde{\rho} = a(\tilde{\mu} - \alpha_2) \quad ; \quad \varphi = 0, \pm \pi, \bullet 2\pi,... \tag{13a}$$

and for $\tilde{\mu} > 0$ at :

$$\tilde{\rho} = a(\tilde{\mu} + \alpha_2) \quad ; \quad \varphi = \pm \frac{\pi}{2}, \pm \frac{3\pi}{2},... \tag{13b}$$

For $\tilde{\mu} = 0$, the density $\tilde{\rho}$ jumps from $-a\alpha_2$ to $+a\alpha_2$ while the anchoring direction jumps from $\varphi = 0$ to $\varphi = \frac{\pi}{2}$ or $\varphi = -\frac{\pi}{2}$.

- $\bar{a}_4 > 0$: The function $\tilde{f}_{tot}$ plotted in Fig. 22b shows only one row of minima, located at $\tilde{\rho} = 0$, $\varphi = \pm \frac{\pi}{4}, \bullet \frac{3\pi}{4},...$

For $\tilde{\rho} < \tilde{\rho}_- = -\frac{a\alpha_2^2 + 4\bar{a}_4}{\alpha_2}$, the grooves are located at $\varphi = 0, \pm \pi,...$ At $\tilde{\rho} = \tilde{\rho}_-$, each groove bifurcates into two grooves following the curves

$$\cos 2\varphi = -\frac{\alpha_2}{a\alpha_2^2 + 4\bar{a}_4}\tilde{\rho} \tag{III.14}$$

At $\tilde{\rho} = \tilde{\rho}_+ = -\frac{a\alpha_2^2 - 4\bar{a}_4}{\alpha_2}$, the same bifurcations occur, from grooves located at $\varphi = \pm \frac{\pi}{2}, \pm \frac{3\pi}{2},...$

Then, the plane $\bar{P}$ is tangent to the surface $\tilde{f}_{tot}$ for $\tilde{\mu} < \tilde{\mu}_- = -4\frac{\bar{a}_4}{a\alpha_2}$ at :

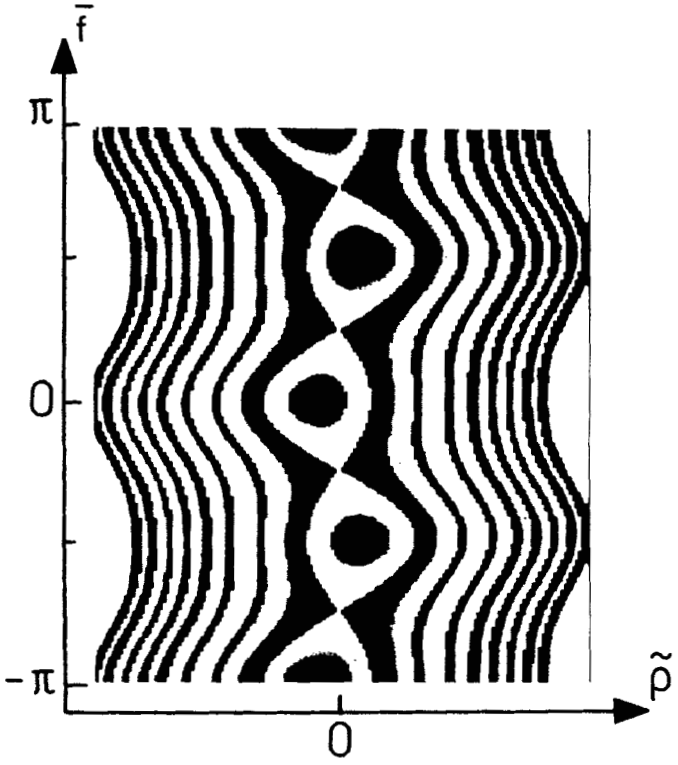

FIGURE 22a, Surface free energy $\bar{f}_{tot}(\varphi,\tilde{\rho}) = f_{iso} + f_a - \mu_c\rho$ in the case when the anisotropic part is given by eq. (III.7). Characteristic of a 1st-order anchoring transition
See Color Plate VIII.

$$\tilde{\rho} = a(\tilde{\mu} - \alpha_2) \quad ; \quad \varphi = 0, \pm\pi, \pm 2\pi, \ldots \tag{III.15a}$$

for $\tilde{\mu} > \tilde{\mu}_+ = 4\frac{\bar{a}_4}{a\alpha_2}$ at :

$$\tilde{\rho} = a(\tilde{\mu} + \alpha_2) \quad ; \quad \varphi = \pm\frac{\pi}{2}, \pm\frac{3\pi}{2}, \ldots \tag{III.15b}$$

and for $\tilde{\mu}_- < \tilde{\mu} < \tilde{\mu}_+$ at :

$$\tilde{\rho} = (a + \frac{(a\alpha_2)^2}{4\bar{a}_4})\,\tilde{\mu} \quad ; \quad \cos 2\varphi = -\frac{\alpha_2 a}{4\bar{a}_4}\,\tilde{\mu} \qquad \text{(III.15c)}$$

The transition between the orientation $\varphi = 0$ and $\varphi = \pm \frac{\pi}{2}$ is continuous.

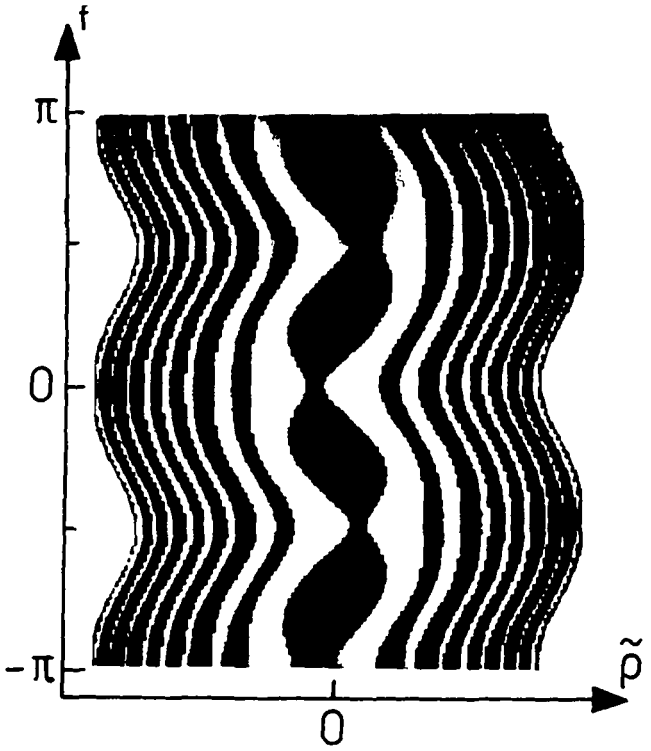

FIGURE 22b, Surface free energy $\tilde{f}_{tot}\ (\varphi,\tilde{\rho}) = f_{iso} + f_a - \mu_c\rho$ in the case when the anisotropic part is given by eq. (III.7). Characteristic of a 2nd-order anchoring transition
See Color Plate IX.

IV. DISCUSSION

Adsorption-induced anchoring transitions involve modifications of surface excess densities ρ_i of chemical species having a reanchoring action. The experiments reported in this article point out that water is the first example of such reanchoring substances. Other chemicals, for example alcohols, also show reanchoring action. The effect obtained with alcohols depends on their

structure. For example, ethyl alcohol CH_3 CH_2 OH not only induces anchoring transitions but also modifies wetting conditions while ethylene glycol OH CH_2 CH_3 OH, which has two OH groups, preserves perfect wetting of the crystal substrates by the nematic E9.

The common characteristics of water and of different alcohols is their capacity to form hydrogen bonds. If a molecule of water is hydrogen bonded both to the substrate and to the nematic molecules one can conceive that in such a situation the orientation of the nematic molecule can be different from that which would occur if the nematic molecule interacted directly with the substrate.

The microscopic mechanism of adsorption and reanchoring is related to the problem of reversibility of the anchoring transition. For example, the last two anchoring transitions (Fig. 9) at the E9/muscovite interface occur and are reversible only for one hour following the preparation of the sample, while the first transition, persists for 24 hours. At E9/gypsum and E9/phlogopite interfaces, the anchoring transitions persist for a week or more. In all these cases, the persistence time can be considerably extended by using alcohols as coadsorbents.

Knowledge of the structure and of the composition of freshly cleaved surfaces is also necessary for solving the problems opened by the anchoring transition. The long section devoted to the structure of micas is a first attempt to understand better why the anchoring transitions are so different on different micas. Many other minerals shown to exert the anchoring action should also be tested for the occurrence of anchoring transitions.

The choice of the nematic materials also seems to be very important. Pure products instead of mixtures should be tested.

Can the anchoring transition occur in other mesophases ? One can expect that in smectics, where layers should be rearranged when the director orientation changes, the anchoring transition should exhibit special and unusual features.

Acknowledgments

We wish to thank all persons who have offered us samples of minerals :

– P. Aymard for gypsum crystals,

– B. Platevoet for samples of phyllosilicates,

– Mme J. Briot (Comptoir des Minéraux et Matières Premières) and

– Société Metafix for samples of micas and vermiculites.

We have greatly benefited from discussions with B. Platevoet on structures of minerals and with P. Pfeuty and Mme Noguera on adsorption phenomena.

One of us (P.Pieranski) is grateful to the Organizers of the Conference for their kind invitation to Torino.

REFERENCES

1 An excellent introduction to surface thermodynamics can be found for example in : Films on Solid Surfaces by J.G. Dash, Academic Press, (1975)
2 P. Pieranski and B. Jérôme "Adsorption-induced anchoring transitions at nematic/crystal interfaces", submitted to Phys. Rev. A
3 C. Mauguin, Bull. Soc. Fr. Min. Crist 34, 71 (1911)
4 F. Grandjean, Bull. Soc. Fr. Min. Crist. 39, 164 (1916)
5 L.M. Blinov, E.I. Kats, A.A. Sonin, Sov. Phys. Usp. 30, 604 (1987)
6 W.A. Wooster, Z. für Krist. 94, 375 (1936)
7 S.W. Bailey in Micas, Review in Mineralogy 13, Mineralogical Soc. of Am.
8 K. Müller and C.C. Chang, Surf. Science 14, 39 (1969)
9 This fact is well known since the work of Mauguin and Grandjean. More informations can be found in the textbook by G. Friedel Leçons de cristallographie, Librairie Scientifique Albert Blanchard, Paris (1964)
10 R. Paudit, M. Schick, M. Wortis, Phys. Rev. B 26, 5112 (1982)